NASA/TM–20240007419

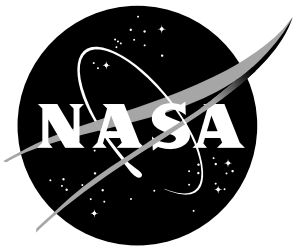

LED Intensity Decay Particle Tracking Velocimetry

Joshua M. Weisberger and Brett F. Bathel
Langley Research Center, Hampton, Virginia

July 2024

NASA STI Program Report Series

Since its founding, NASA has been dedicated to the advancement of aeronautics and space science. The NASA scientific and technical information (STI) program plays a key part in helping NASA maintain this important role.

The NASA STI Program operates under the auspices of the Agency Chief Information Officer. It collects, organizes, provides for archiving, and disseminates NASA's STI. The NASA STI Program provides access to the NASA Aeronautics and Space Database and its public interface, the NASA Technical Report Server, thus providing one of the largest collection of aeronautical and space science STI in the world. Results are published in both non-NASA channels and by NASA in the NASA STI Report Series, which includes the following report types:

- TECHNICAL PUBLICATION. Reports of completed research or a major significant phase of research that present the results of NASA programs and include extensive data or theoretical analysis. Includes compilations of significant scientific and technical data and information deemed to be of continuing reference value. NASA counterpart of peer-reviewed formal professional papers, but having less stringent limitations on manuscript length and extent of graphic presentations.
- TECHNICAL MEMORANDUM. Scientific and technical findings that are preliminary or of specialized interest, e.g., quick release reports, working papers, and bibliographies that contain minimal annotation. Does not contain extensive analysis.
- CONTRACTOR REPORT. Scientific and technical findings by NASA-sponsored contractors and grantees.
- CONFERENCE PUBLICATION. Collected papers from scientific and technical conferences, symposia, seminars, or other meetings sponsored or co-sponsored by NASA.
- SPECIAL PUBLICATION. Scientific, technical, or historical information from NASA programs, projects, and missions, often concerned with subjects having substantial public interest.
- TECHNICAL TRANSLATION. English-language translations of foreign scientific and technical material pertinent to NASA's mission.

Specialized services also include organizing and publishing research results, distributing specialized research announcements and feeds, providing information desk and personal search support, and enabling data exchange services.

For more information about the NASA STI Program, see the following:

- Access the NASA STI program home page at `http://www.sti.nasa.gov`
- Help desk contact information: `https://www.sti.nasa.gov/sti-contact-form/` and select the "General" help request type.

NASA/TM–20240007419

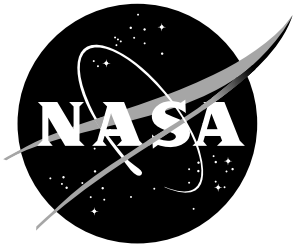

LED Intensity Decay Particle Tracking Velocimetry

Joshua M. Weisberger and Brett F. Bathel
Langley Research Center, Hampton, Virginia

National Aeronautics and
Space Administration

Langley Research Center
Hampton, Virginia 23681-2199

July 2024

Acknowledgments

The authors would like to thank Nicholas Stumpo and Stephen Jones for their assistance with the LED circuitry and setup, Scott Bartram and Jian Gao for the use of, and help with, the particle seeding system, Wayne Page for improvement to the particle seeding system, Paul Danehy and Ross Burns for helpful discussions, Jenna Eppink for exploration of preliminary testing opportunities, and Scott Bartram and Jenna Eppink for clarifying revisions to the paper. The work was funded by the NASA Transformational Tools and Technologies (TTT) project.

Available from:

NASA STI Program / Mail Stop 050
NASA Langley Research Center
Hampton, VA 23681-2199

Abstract

A particle tracking velocimetry (PTV) system is demonstrated that eliminates the need for expensive lasers and cameras, and encodes the particle tracks with a known intensity variation which allows for high-resolution particle velocity and directionality determination. Using a light-emitting diode (LED) as the light source significantly reduces cost and allows for eye-safe operation, in comparison to traditional laser systems. The intensity variation control is passive, being dictated by the capacitance discharge rate in the LED pulsing circuit. The decay rate can be adjusted with the LED circuit capacitors/resistors, while the duration of the decay can be adjusted with the LED trigger pulse width. Because the intensity decay illumination is controlled by the LED, a single long exposure camera image is used to acquire images of the particle streaks, and there is no need for a more complicated and costly double-pulsing camera. With the intensity coding of the light, a single-camera/single-LED system can identify particles entering of leaving the illumination plane, but cannot discern the direction toward or away from the camera. By using a two-color system, three-dimensionality of the particle tracks can be determined.

1 Introduction

Particle image velocimetry (PIV) is a well-established optical diagnostic for the measurement of flow velocity, and comprehensive overviews of the operating principles can be found in Refs. [1–4]. Generally, a light source is formed into a sheet with a combination of spherical and cylindrical optics (typically called "sheet-forming optics" in many publications) and illuminates a flowfield of interest. This flowfield is seeded with small particles that are nearly neutrally buoyant such that they follow the local direction of the flow. A camera, placed orthogonal to the plane of the light sheet in a simplified setup, captures images of the particles illuminated by the light through scattering. Typically, to obtain the velocity of the flowfield, the light source and camera are synchronously double-pulsed in quick succession, acquiring two images of the particle field at two closely separated instances in time. These two images are then compared, often using a cross-correlation or optical flow algorithm, and the velocity field is obtained. To achieve high intensity, light uniformity, and accurate pulsing control, lasers are often used as the light source. However, light-emitting diode (LED) light sources have also found use [5–10]. Because particles are made visible by a sheet of light, conventional PIV systems are inherently two-dimensional, limited to the plane of illumination. Stereoscopic PIV uses a second camera to resolve the out-of-plane component of the velocity [11–13]. Examples of other three-dimensional PIV techniques are scanning PIV, defocusing PIV, holographic PIV, tomographic PIV, and synthetic aperture PIV [4, 14]. Moving from the basic 2D PIV system to stereo or 3D PIV can require substantial effort.

When the pulse width of the light source and exposure of the imaging system are deliberately increased to record streaks of each particle (akin to motion blur in long exposure images), the technique is typically called particle streak velocimetry (PSV), particle streak tracking (PST), or particle tracking velocimetry (PTV), among other

similar names; the acronym of PTV will be used for the remainder of this paper for clarity. Streak imaging has been used extensively as a diagnostic for many decades, but only a selected history of its use will be provided here for conciseness (for further reading, see Refs. [15–19]). In the early 1980s, Dickey *et al.* extended streak photography to velocity measurements, and noted in their abstract that it "requires only limited technical resources", a benefit of this simple technique [20,21]. The exposure of the light source was controlled using a spinning chopper wheel, and pieces of mylar were used on this wheel to change the transmitted intensity of the light over the exposure duration to define the particle motion direction (short and long bright sections separated by a dim section). The head and tail of the streaks, along with the time separation known from the chopper wheel rotation, were used to determined the velocity. In 1981, particle streak images were acquired on film using a long exposure of 125 ms on 35 mm film in Ref. [22]. In 1989, Cenedese *et al.* used color-coding of a multi-exposure photograph to determine the third component of velocity, using two parallel light sheets of different colors [23]. In 1989, Khalighi and Lee used intensity-coded laser pulses to determine the direction of the particle tracks, and developed an automatic image processing algorithm to determine the velocity vectors from the images [24]. In 1992, Dinkelacker *et al.* used a similar method to determine the third velocity component, this time using a single light sheet that was color graded over its thickness [25]. The light sheet had an exponentially decaying intensity profile over its thickness (perpendicular to the sheet), and only a single laser light wavelength and single monochrome camera were used for the imaging. Other examples of using overlapping light sheets to determine the third velocity component, for PIV instead of PTV, include work by Raffel *et al.* [26] and Brucker *et al.* [27]. Towers *et al.* demonstrated the use of fluorescent particles for two-color PIV measurements, allowing for unambiguous flow direction with multi-wavelength illumination for both fluorescent and non-fluorescent seed particles for two-phase flows [28].

Lasers had typically been used for PIV/PTV measurements due to their high intensity, narrow wavelength, and pulsing/syncing ability with imaging systems. As LEDs became widely available, they found immediate use in PIV/PTV systems. Chételat *et al.* used LEDs as an inexpensive alternative to lasers, with random pulsing on/off patterns to determine directionality of the particles [5]. They note that these LEDs were smaller, cheaper, easier to handle, and less hazardous than other PIV systems. However, they also note that thin sheets of light (like those attainable with lasers) were not feasible, so volume illumination was used (where the camera/imaging system determines the depth-of-focus, not the light sheet). Estevadeordal *et al.* used LED lights for shadow PIV, with intensity pulse shape examples shown in Fig. 7 of their paper [6]. This method is close to that proposed here, but the authors only noted that the longer exposures produce streaks, and that they have directional ambiguity. In 2008, Hagsaeter *et al.* used LED illumination for micro-PIV and front-lit configurations, again using volume illumination instead of sheet illumination [7]. They discuss the benefits of using LED illumination, including: small size, adaptability to different fluorescent dyes, incoherent light, freely adjustable pulse length and repetition rate, low energy consumption, and low cost. Jehle *et al.* used an LED PIV system to determine the third velocity component

by using absorption of the light through a liquid to provide the particle depth information [29]. High-quality LED PIV data was achieved by Willert *et al.* using an over-driven LED (i.e., short-duration electric current supplied at a level that exceeds that used during continuous operation) to provide high intensity light, past what is typically available for LEDs [8]. It is this method of LED operation that the work discussed in this paper is based off of, using a modified version of the driving circuit discussed by Willert *et al.*; this modified LED driving circuit was used in the tomographic background-oriented schlieren work presented in Ref. [30]. Representative time traces of the LED pulses are shown in Fig. 2 of Ref. [8], although the intensity decay demonstrated at longer pulse widths was not used for PTV. Buchmann *et al.* used high-power LEDs as light sources for their tomographic PIV measurements, and show the typical intensity decay of the LED pulse in their Fig. 2b, although this intensity decay was not utilized [9]. Raffel *et al.* have recently explored the use of an in-line forward scattering illumination method for PIV/PTV using a variety of imaging configurations with LED light sources [31].

Phosphor particles have found use in PIV/PTV measurements to measure both velocity and temperature due to their known decay profiles with certain UV illumination. One benefit of phosphor decay times is that dual sensing of velocity and temperature of the particle streaks can be determined [32–34]. In Ref. [32], a high-speed camera took sequential images of the luminescence decay as the particles moved, where the velocity vector was determined from the movement of the particles in the sequential frames, and the temperature was determined from the intensity decay from frame-to-frame using knowledge of the camera frame rate.

The previous studies most similar to the work presented in this paper use long-exposure streak imaging to determine velocity and direction [22, 35–37]. The most similar method is by Voss *et al.* [35], where a two-color intensity modulation LED PTV system was demonstrated. This system used an LED as the light source (eliminating the need for a laser), used a long exposure of a typical camera (eliminating the need for an expensive high-frame-rate camera), and used intensity modulation of the LED to code directionality of the particles. However, the experimental setup in Ref. [35] still required a driving circuit for the intensity modulation. Another similar measurement technique is that outlined by Fan *et al.* in Refs. [36, 37], where phosphor decay particle streaks were used to determine velocity magnitude and direction of phosphor particles. The limitation of this work is that the decay times of the phosphor particles are fixed by the particle composition, and so particles are specifically tailored for certain flow velocity regimes.

The system outlined in this paper can be thought of as quasi-combination of the techniques in Refs. [35–37]. The primary benefit of this proposed system is that the intensity modulation is passive, a natural byproduct of the capacitance discharge in the LED circuit itself. This decay can be changed by adjusting the capacitance and/or resistance in the LED circuit quite easily. Further, specially made particles are not required, the intensity decay profile can be changed, and active modulation of the LED illumination is not required. A single camera, single LED system can adequately resolve the varying velocity field in complex flows, and if three components of the velocity are required, a two-color system can be used with either one color camera or two monochrome cameras with a dichroic mirror.

2 LED Intensity Decay

The idea for the use of the LED intensity decay originated from a high-speed schlieren measurement of an expanding shock wave, where the LED circuit followed the design of Willert *et al.* [8]. An example of the intensity decay of the LED light source is shown in Fig. 1a, where five selected frames from an image sequence are shown, and where the intensity can be seen continuously decreasing from frame 25 to frame 225. By taking a mean image intensity for every frame in the image sequence, the intensity decay curve can be plotted in Fig. 1b. This curve shows the non-linear, yet monotonic, decay of the emitted light intensity over a certain period of time, which can be seen to be exponential with the plotted dashed cyan exponential curve fit to the raw data. The repeatability of this decay curve was demonstrated to be very high (not shown here), although this repeatability is not a requirement for the system proposed here because the intensity is continuously monitored for every image acquisition.

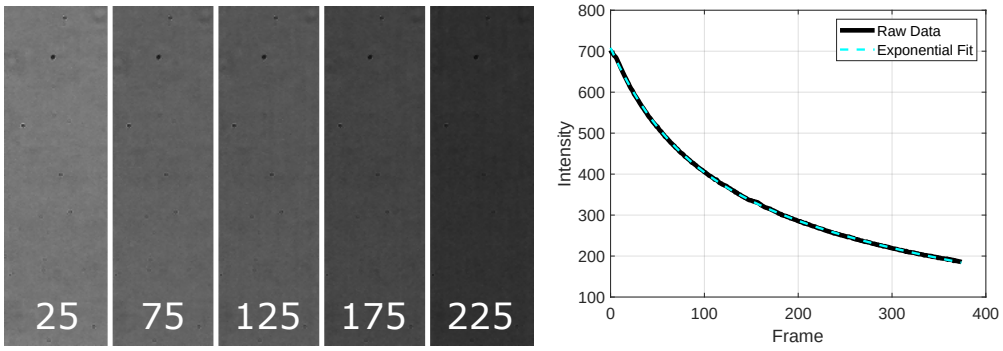

(a) (b)

Figure 1: (a) LED intensity decay images from a high-speed schlieren system with frame number identified, and (b) mean pixel intensity versus image number (solid black) and exponential decay curve fit (dashed cyan).

As mentioned in Section 1, other authors that have used LEDs as the illumination source in their work have shown the intensity decay of the emitted LED light, but have not utilized it for streak imaging. In Fig. 7b of Ref. [6] (reproduced schematically here in Fig. 2a), a 1 μs pulse exhibits a relatively slow rise time and an exponential decay time. The pulse used here is short, however, and the decay time is fast. This same LED pulse output trend can be seen in Fig. 2a of Ref. [9] (reproduced schematically here in Fig. 2b) for a 10 μs pulse, where the bottom trace is the input TTL pulse to the LED, the middle trace is the current pulse, and the top trace is the measured light output signal from a fast photodiode. In the top trace, similar rise and fall characteristics of the light output are visible as in Fig. 2a. The best example of the useful intensity decay signal from a pulsed LED can be seen in Fig. 2b of Ref. [9] (reproduced schematically here in Fig. 2c). The decaying light intensity from a single pulse of 150 μs (factor of 15 increase in pulse

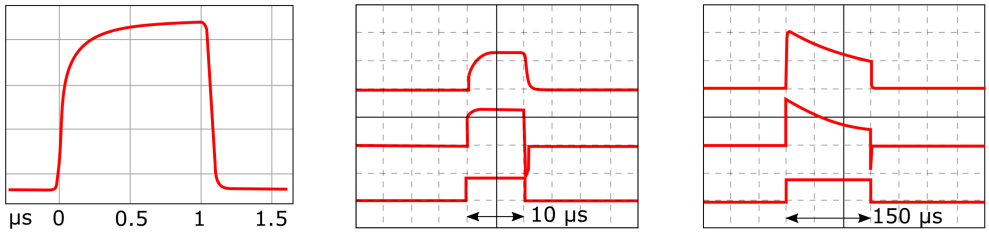

(a) (b) (c)

Figure 2: Examples of measured intensity output from pulsed LEDs for pulse widths of (a) 1 μs [Ref. [6]], (b) 10 μs [Ref. [9]], and (c) 150 μs [Ref. [9]]. In (b) and (c), the bottom trace is the input TTL pulse, the middle trace is the measured current pulse, and the top trace is the light output measured by a photodiode. Figures are schematic representations of the original figures.

width from Fig. 2b) of an LED is visible, but note that this paper does not utilize this intensity decay for streak imaging, instead using the overall light emitted from the pulse for the conventional double-pulsing PIV measurements.

3 Experimental Setup

3.1 Single-Color Operation

A schematic of a single-color system is shown in Fig. 3. The light source depicted is a red LED which outputs a defined intensity profile in time, where the total duration of the decay is determined by the input TTL trigger duration (i.e., pulse width). A pick-off mirror (M) reflects a small portion of the light to a detector to be used as an intensity monitor. The transmitted light passes through a lens to form an image of the LED element at the measurement location (here, a low velocity jet with 1 μm particles in the flow). A monochrome machine vision camera views the flow of interest from a nearly-forward-scattering orientation to achieve the highest signal intensity. Because the light illuminates the entire volume of the particle jet, the narrow depth-of-focus of the imaging plane is achieved through appropriate combination of the camera, lens, and extension tubes. This type of imaging strategy is used in Refs. [7, 31, 38], where the imaging plane is determined by the imaging system depth-of-focus, not the illumination sheet thickness. Note, however, that any imaging angle can be used provided the illumination intensity and camera sensitivity are sufficient to acquire high enough pixel intensities of the particles over their streak duration.

A simplified schematic of the single-color system is shown in Fig. 4a, now with the camera imaging the orthogonally scattered light from the LED (note that beam-forming optics are not depicted here, but a system similar to that shown in Fig. 10 of Ref. [8] can be used). The intensity decay profile, $I(t)$, of the LED measured by the detector is shown in Fig. 4b, exhibiting the monotonic exponential decay in time. The duration of this intensity decay in time is dictated by the desired pulse

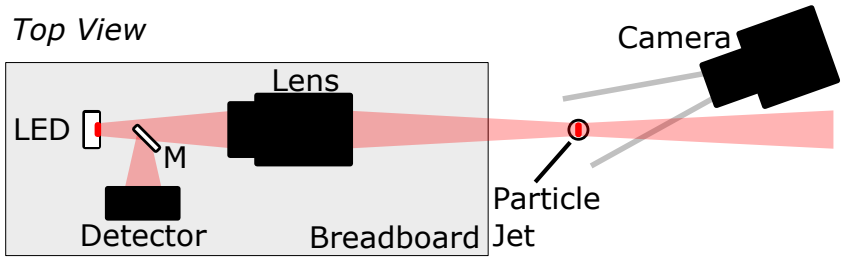

Figure 3: Schematic of the single-color LED intensity decay PTV system, where M is a small pick-off mirror to measure the intensity decay of each LED pulse. The camera images forward-scattered light from the particles to maximize the intensity.

width of the LED, which is set using an input TTL pulse to the LED circuit, whereas the decay rate within this pulse width is dictated by the LED circuit's design, and most influenced by its resistance and capacitance.

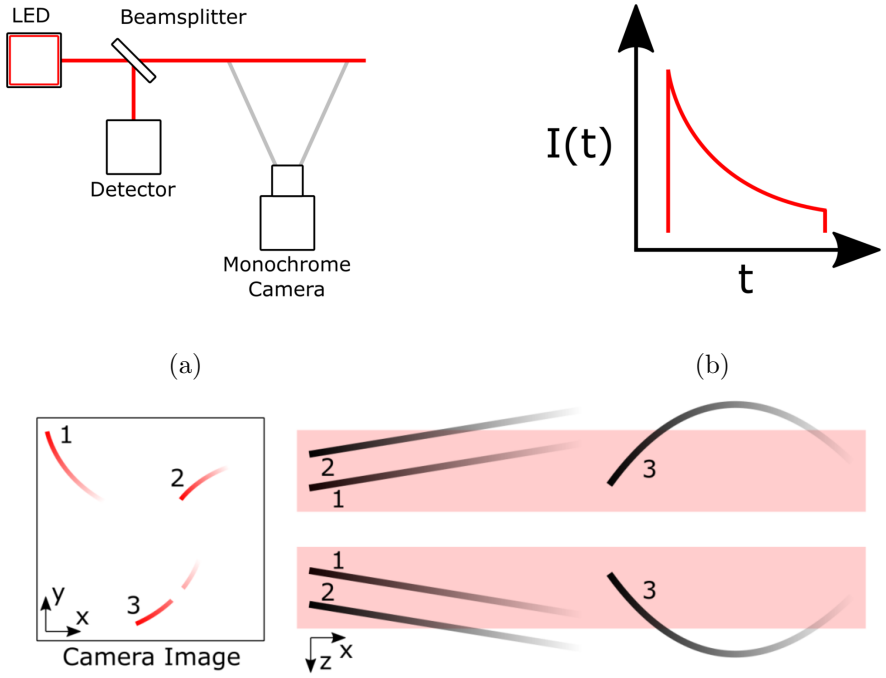

Figure 4: (a) Simplified schematic of single-color system viewing the LED light sheet from the side (90° scatter), (b) LED pulse intensity decay profile, and (c) three characteristic particle streaks shown in the camera view (left) and from a top-view of the LED sheet (right).

A representative camera image with three (of many) possible measured particle streaks is shown in Fig. 4c on the left. On the right of Fig. 4c, a top-view of the LED light sheet is shown in red, with the correspondingly-numbered particle streaks

denoted. For streak 1, the particle remains within the thickness of the illumination sheet over the duration of the pulse width, Δt, and the full streak is captured on the camera sensor. For streak 2, the particle exits the illumination sheet before the pulse concludes, and so the streak appears shortened in the camera image. Note also that the particles can enter the sheet instead of exiting the sheet, but the intensity profile will indicate which of these occurs. For streak 3, the particle exits the illumination sheet, and then re-enters a short time later. This shows up on the camera image as a particle streak with a missing section in the middle. For these sheets of finite thickness, note that the velocity of streak 1, for instance, will be under-predicted due to its projection onto the camera's x-y plane, which appears as a shorter streak than it actually is in physical space. The two top-view images of the illumination sheet and streaks in Fig. 4c (right) are equally valid scenarios for the images acquired by the camera in Fig. 4c (left). To avoid this directional ambiguity, a two-color system can be used.

3.2 Two-Color Operation

While single-frame (longer exposure) imaging can provide high-quality, easy to interpret images, Ref. [1] notes that "*...in three-dimensional fields, foreshortened image streaks are created when particles enter or leave the light sheet during the exposure...*". This third component of velocity can be determined by using color-coding of adjacent light sheets, as was demonstrated in Ref. [23]. If the measurements are being performed in liquids, absorption of different wavelengths of light through the liquid when scattered by the suspended particles can provide information on the third component of velocity [29]. In the single-color system described in Section 3.1, the directional ambiguity of particle streaks using a single color was exemplified in the schematic of Fig. 4. If only a single-color system is used, particle streaks that are shorter than the duration of the LED pulse can simply be discarded during a pre-processing validation step. However, if the out-of-plane particle streaks are desired, then a two-color system like that described in this section can be used. Note that when using volumetric illumination such as is typical for the LED systems described here, a third component of velocity may also be obtained using a single LED system with two cameras, each focused on a narrow plane offset from one another, and performing a volumetric calibration to determine the particle position.

The LED intensity decay PTV system is ideally suited for expansion to a two-color (or multi-color) system, with the only additions being more low-cost LED units and associated optics. A schematic of the two-color system is shown in Fig. 5, where the configuration of the optics for both red and blue LED portions of the system are the same, and follow the design of the single-color system shown in Fig. 3. Here, a red and a blue LED are used, and reflected by turning mirrors to provide precise angular adjustment of the reflected beams to align them optimally above the particle jet, approximately adjacent to one another. A top-view image of the red and blue light sheets is shown at the top-right of Fig. 5, where the light is made visible in this image using a piece of paper to show the focusing light rays.

To demonstrate its operation, a simplified schematic of the two-color (red/blue) system is shown in Fig. 6a, where the light from the two LEDs is initially split by a

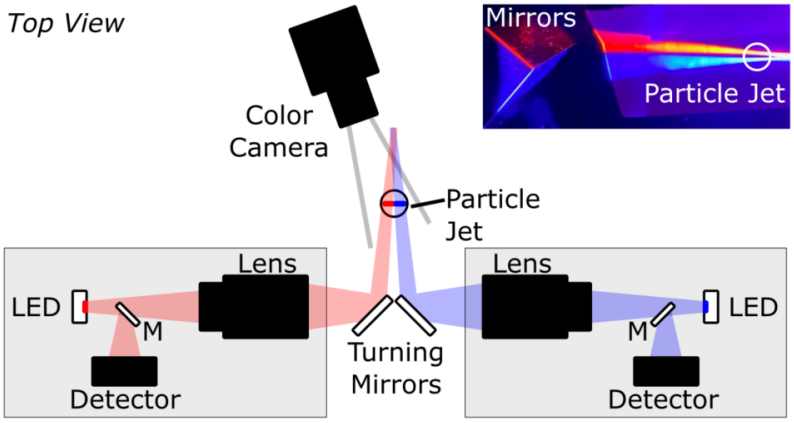

Figure 5: Schematic of the two-color system using a single color camera, and top-view image of the mirrors and red/blue light sheets adjacent to one another above the particle jet (light made visible using a piece of paper).

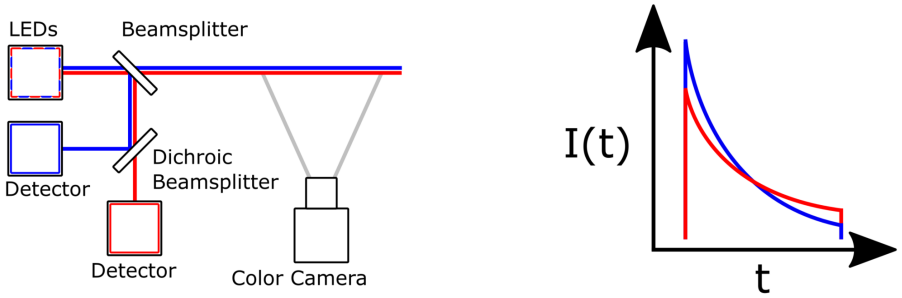

(a) (b)

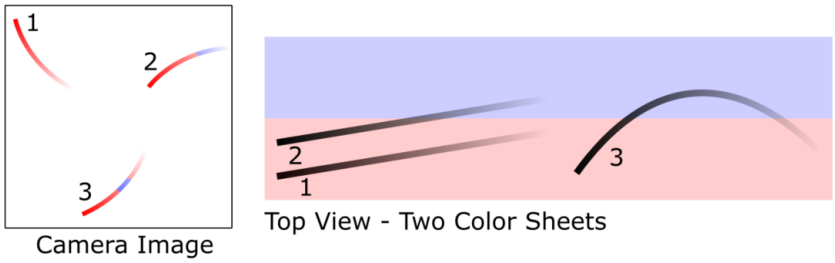

(c)

Figure 6: (a) Simplified schematic of two-color system viewing the LED sheet from the side (90° scatter), (b) LED pulse intensity decay profiles, and (c) three characteristic particle streaks shown in the camera view (left) and from a top-view of the LED sheets (right).

beamsplitter, with a portion being reflected and the remaining light transmitted as two adjacent planes to the flow region of interest, which is viewed orthogonally by a color camera. The reflected light is split by a dichroic beamsplitter (longpass in this schematic), with the blue and red light detected separately by two photodiodes to measure their intensity decay. These intensity decay profiles are shown in Fig. 6b, noting that the two LEDs need not have the same decay rate, since both are recorded simultaneously. The duration of the two pulses is the same in this image, although this is also not a fixed requirement given two separate TTL pulses are supplied to the two LEDs, and the camera exposure is longer than the longest LED pulse width. The utility of the two-color system compared with the single-color system is shown in Fig. 6c, with a camera image of three (of many) possible characteristic streaks shown at the left, and the top-view of the adjacent illumination sheets at the right; the three streaks are the same as those shown in Fig. 4c. For streak 1, the imaged streak on the camera is the same as shown in Fig. 4c because the particle remains within the confines of the red sheet. For streak 2, the first part of the imaged streak is red, and then transitions to blue as it passes out of the red sheet and into the blue sheet. For streak 3, the camera image shows the streak passing from the red to the blue and back to the red sheet, and the directionality of the particle over its streak duration is evident.

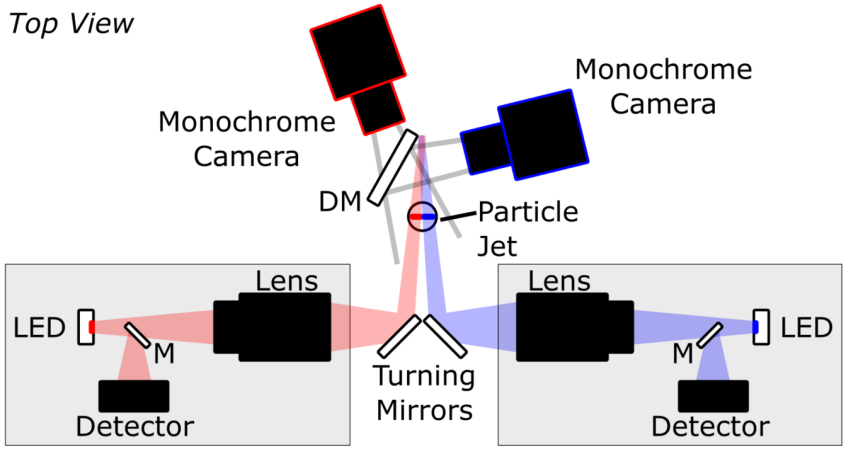

Figure 7: Schematic of the two-color system, where two monochrome cameras are used to increase imaging resolution/quality, and both view the same scattering angle and field-of-view through the use of a dichroic mirror (DM).

The color camera setup of Fig. 5 may result in imaged streaks that are of lower quality than when using a monochrome camera, typically due to the color mask present on the sensors of color cameras. To increase the resolution and quality of the two-color system, the configuration shown in the schematic of Fig. 7 can be used, where a dichroic mirror is used to split the scattered light from the blue and red LEDs to be imaged by two monochrome cameras, each viewing the same scattering angle and field-of-view through the use of the dichroic mirror, DM. A single monochrome camera can also be used in place of the color camera if it is clear from a pre-run calibration which parts of the image correspond to each LED's

illumination. This is relatively simple if the intensity decay profiles of the two LEDs are sufficiently different, which will be shown in the results of Section 5.3.

4 Image Processing

The simplest method of processing conventional PIV images is to use a two-frame cross-correlation method. Two images are acquired by double-pulsing both the light source and the imaging camera, with a precisely known delay time between the first and second pulse/image. A windowed cross-correlation calculation results in estimated 2D velocity vectors in the imaging plane, albeit at a lower resolution than the initial images due to the windowing necessary for the processing method. Further details of this processing method can be found in Refs. [1, 4, 39].

To obtain the necessary velocity information of the particle streaks in the images, other processing steps are required beyond the typical cross-correlation method. The simplest option for streak processing is to treat the start and end point of the streaks as the two "frames" from a conventional double-image PIV test, since the streak duration time is known (akin to the dual-pulse offset in traditional PIV measurements). The velocity vector calculated from these data then ignores the path of the particle between the start and end of the streak, omitting useful information about the flow. Since the imaged intensity decay streaks are exponential in nature due to the capacitor discharge, the processing methods outlined in Refs. [36, 37] can be used. Yet another option for streak processing can be found in Refs. [35, 40].

To obtain the most information from the streak images, the streaks first need to be identified in the image. Manual identification is possible but time-consuming. Edge detection or image segmentation algorithms can be used to automatically find streaks in the images instead of manually selecting them. An example of a raw image is shown in Fig. 8a, with automatically identified streaks shown in Fig. 8b.

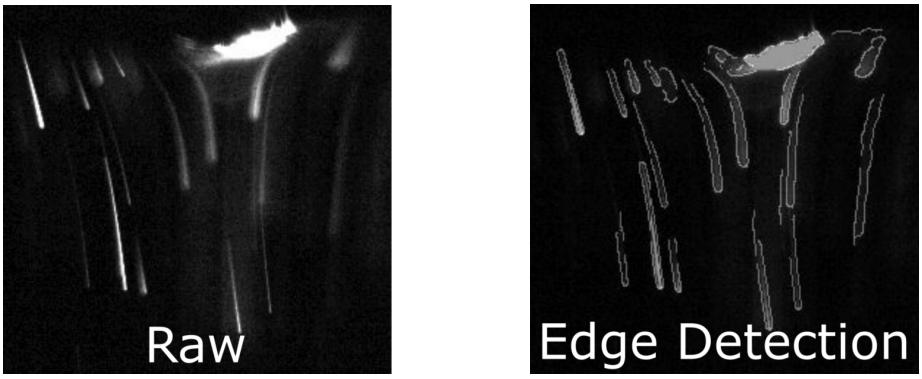

(a) (b)

Figure 8: Images of (a) raw particle streaks and (b) automatic edge detection of the identified particle streaks, which can be used to automatically extract intensity decay profiles of the particle streaks.

Using these identified regions, the intensity profile from beginning to end of each streak is extracted, and can be used with the known (measured) intensity decay for that image frame. Note, however, that both in-focus streaks at the left of the image and out-of-focus streaks at the center/right of the image are identified, and manual adjustment of processing parameters or outlier removal may be needed.

If there are many out-of-focus particles in the image (e.g., due to a higher than expected seeding density), a high-pass filtering of the image can be performed prior to streak identification and intensity extraction, as shown in Fig. 9, to identify particles only at the sharpest plane of focus of the imaging system. Here, a 2D fast Fourier transform (FFT) of the raw image is first computed. To perform a high-pass filtering of the image, an arbitrary circular portion of the FFT image is removed from the center, which corresponds to the lowest frequencies in the image. Finally, the inverse FFT is computed, resulting in the high-pass filtered image at the right of the figure. Comparing the raw and filtered images shows a pronounced reduction in the out-of-focus particle streaks, allowing the in-focus particle streaks to stand out and making the edge detection algorithm more efficient. Note, however, that the out-of-focus particle streaks do in fact contain information about out-of-plane position of the particles, and their position in 3D space can likely be determined with calibration of particle blur versus position away from the plane-of-focus prior to testing.

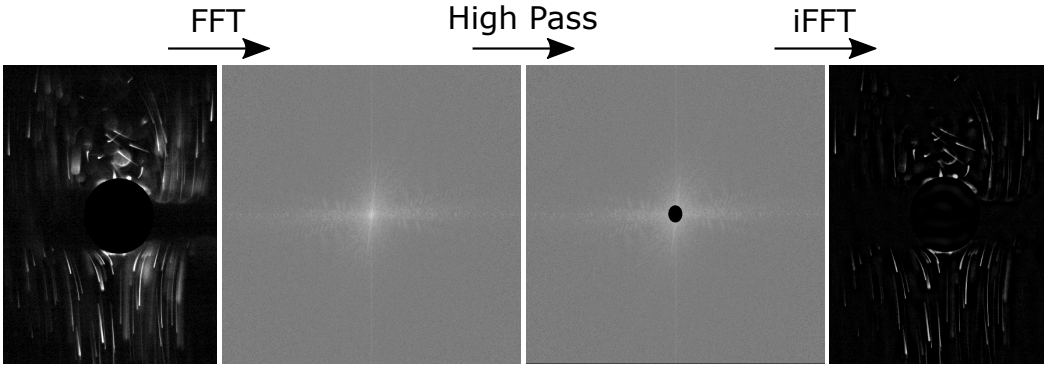

Figure 9: Processing steps used to high-pass filter the raw PTV image to remove background and out-of-focus particle streaks.

The intensity profile across the light sheet will affect the scattered intensity imaged by the camera in a way that changes the recorded intensity decay profile from the actual light decay. For example, if the light sheet has a Gaussian profile across its width, then a particle moving from the middle of the sheet to the edge of the sheet will exhibit a Gaussian decay of its intensity that is independent of its scattered intensity decay profile, $I(t)$. This can be accounted for by taking a sheet-intensity calibration image prior to the experiments, and adjusting the recorded images by this calibration image. An example of this effect being used deliberately is the intensity-graded light sheet used in Ref. [25].

5 Results and Discussion

5.1 LED Pulses

Both red (PT-120-RAX) and blue (PT-120-B) LEDs were connected to the driving circuit board which was powered by a 12 V DC power supply, and a trigger source provided a TTL pulse whose width defined the duration of the streak illumination. For the testing discussed in the following sections, LED pulse widths of either 100 μs, 200 μs, or 300 μs were used. The time traces of the three pulse widths for the blue and red LEDs are shown in Fig. 10a, where the traces have been offset vertically for better visual comparison.

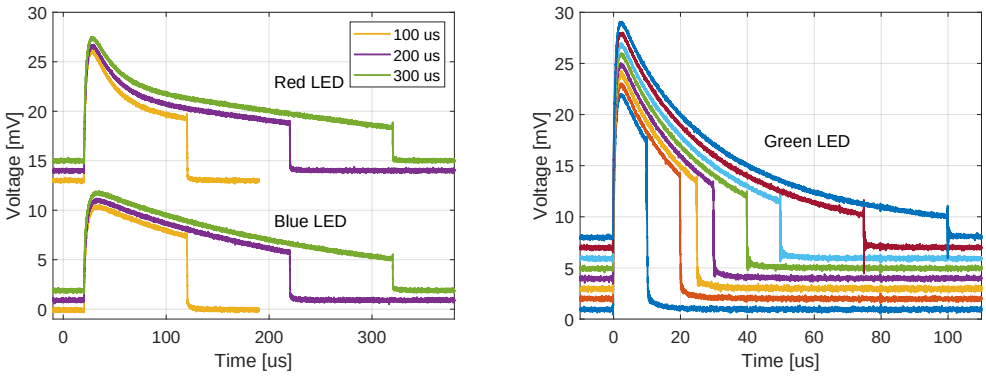

(a) (b)

Figure 10: (a) Red and blue LED intensity decay profiles for three pulse widths of 100 μs, 200 μs, and 300 μs (measured by the photodiodes shown in Fig. 5). (b) Green LED intensity decay profiles for various pulse widths. Traces in both plots are offset vertically for clarity.

These intensity decay traces are similar to the top trace of Fig. 2c, which shows the intensity decay from Ref. [9] with a 150 μs duration. With different resistors and capacitors included in the pulsing circuit design, different decay profiles can be achieved. For example, the decay profile from the blue LED shows a more gradual decrease in intensity than the red LED, a result of a different capacitor used between the two circuits. Each of the three pulse widths used and plotted in Fig. 10a ensure that the LED intensity does not decrease to a value too close to the "off" intensity. This is to maintain the scattered streak signal at a level that can still be imaged by the camera with a high enough signal-to-noise ratio, and also to provide a definitive end-point to the streak such that the rudimentary start-to-end point processing discussed in Section 4 can be used to give an initial estimate of the velocity field.

For higher speed flows, these pulse width durations (and thus streak lengths) may be too long. By changing the capacitance values of the circuit, the decay rate can be increased, as shown in Fig. 10b. Here, a green LED (PT-120-G) was used for the illumination, with data traces acquired for eight pulse widths (10, 20, 25, 30, 40, 50, 75, 100 μs), and which are offset vertically for clarity. Because only the pulse

width was changed between data sets and not the capacitance of the circuit, the general decay profile is the same for all pulse widths, only truncated for the shorter pulse widths. These differences in decay profiles and decay times demonstrate the versatility of the illumination source, although the resistance/capacitance of the circuit should be tailored to the expected flow velocities of the experiment. For example, the optimal decay profile may depend on the camera imaging magnification, the mean flow velocity, the seeding density, etc.

5.2 Qualitative Single-Color Results

As an initial qualitative demonstration, the single-color system (using a red LED) shown in the schematic of Fig. 3 was used to image the flow from a small 4 mm inner-diameter nozzle, as shown in the cropped image of Fig. 11(a), where flow is from bottom to top. The edge of the nozzle can be identified by the reflection near the bottom of the image. Because the camera depth-of-focus is narrow, there are particles near the front and back of the jet that are out of focus in the images. The sharp particle streaks in the image are those particles that occur in the narrow depth-of-focus of the camera system. The forward scattering configuration of this system resulted in relatively high signal intensity. To demonstrate the utility of the intensity decay illumination for particle direction determination, an opposing jet was placed above the upward-facing jet from Fig. 11(a), facing in the opposite direction, without particles present in its flow. A resulting image from this opposing jet flow is shown in Fig. 11(b), with three labeled particle streaks showing different

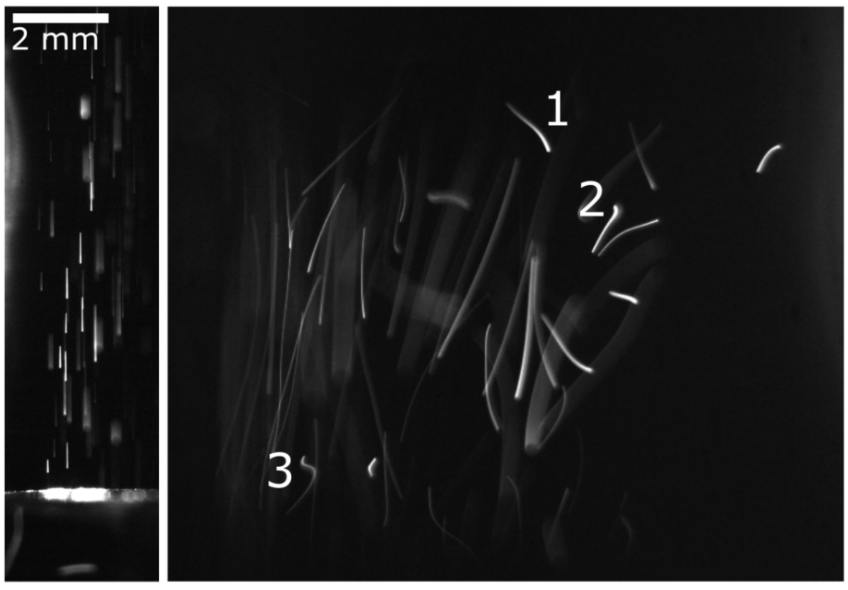

Figure 11: Raw single-color LED monochrome images of (a) freestream flow from a jet (flow bottom to top) and (b) chaotic region of opposing jet flow. Images are cropped from full size of roughly 19.5 × 12 mm.

characteristics. Streak 1 is moving towards the top-left of the image, whereas streak 2 is moving towards the bottom-left of the image, based on their intensity decay profiles. Streak 3 exhibits an 'S' shape, where the direction of the particle changes multiple times within the pulse duration. Other characteristics of the flow that can be visually identified from this image are that the longer streaks near the left side of the image are moving faster than the shorter streaks near the right side of the image, because the entire flowfield is illuminated with light of the same pulse duration. Note, however, that without extracting the intensity decay profiles of the streaks, it is difficult to discern by eye whether the shorter streaks correspond to slower moving particles that are fully encompassed in the illumination sheet or if the particles have prematurely exited the illumination sheet.

If there are regions of the flowfield being measured that have sufficiently different flow velocities, then a single pulse width duration may not be suitable for both regions, and can cause problems during the image processing stages of the analysis. For example, images of the flow around a 1 mm diameter cylinder obstruction are shown in Fig. 12 for three pulse widths (100 μs, 200 μs, 300 μs), where the flow is from the bottom to the top of the image. The edge of the particle jet nozzle can be seen at the bottom of the image, the cylinder near the center, and the bright region from the LED light source in the camera field-of-view near the top right (a result of the forward scattering orientation shown in Fig. 3). The brightness of the image has been increased to more clearly show the particle streaks, even though many of them are saturated.

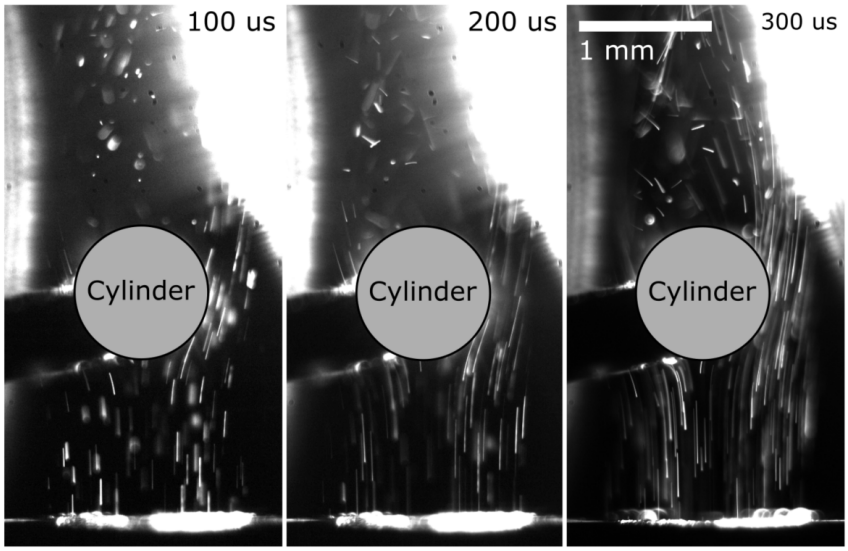

Figure 12: Images of the flow around a cylinder obstruction for three LED pulse widths: 100 μs (left), 200 μs (middle), 300 μs (right). Flow is from bottom to top.

Two distinct regions of flow are visible in these images: the freestream flow below the cylinder and the wake flow above the cylinder. The freestream flow has a higher velocity than the wake flow, and so the particle streaks are long and relatively straight, aside from the region close to the cylinder surface as they begin to curve

around its profile. In the wake, the velocity is low and the particles move in many different directions. In the freestream flow, the 100 μs pulse width provides good quality images of the streaks, without their lengths becoming so long that they interfere with other particle streaks, as can happen with the longer pulse widths of 300 μs. For the wake, the pulse width of 300 μs provides the best particle streaks of these slower moving particles, allowing for high quality determination of both the direction and the velocity of these wake particles. A compromise can be made to obtain adequate imaging of different velocity streaks by using a pulse width of 200 μs, as shown in the middle image of Fig. 12. Both the freestream streaks below the cylinder and the wake streaks above the cylinder have adequate lengths for determination of the velocity profile in the entire image.

5.3 Quantitative Two-Color Results

A two-color system using both a red and blue LED was constructed according to the schematic of Fig. 5. For the results shown below, two configurations of this setup were used, the first using the depicted color camera, and the second replacing the color camera with a monochrome camera. Note that the configuration shown in Fig. 7 using two monochrome cameras with scattered light split by a dichroic mirror could also be used, but was not in these experiments because as shown in Fig. 10a, the intensity decay curves for the red and blue LEDs were different enough such that the light sheets could be differentiated from each other using a monochrome camera by evaluating the extracted intensity decay curves from the image. For these tests, the jet was angled sideways, pointed slightly upwards with flow from left to

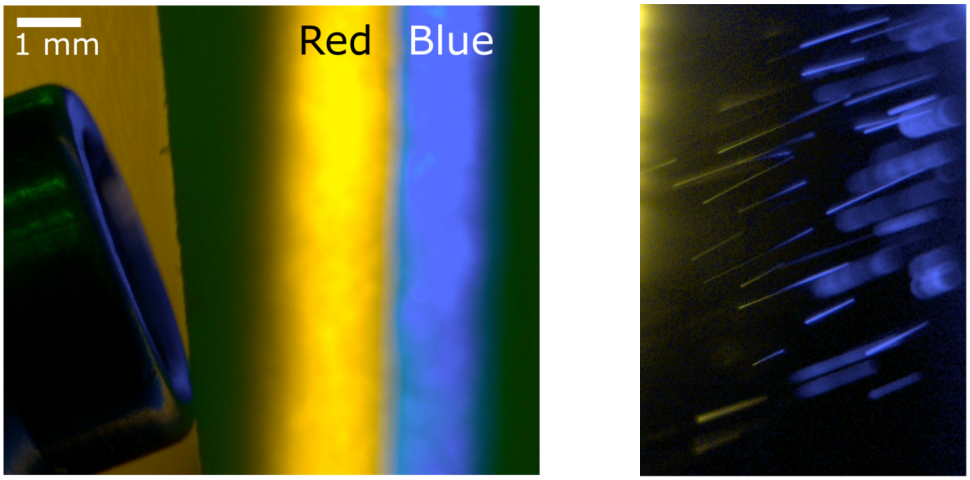

(a) (b)

Figure 13: Color camera images of two-color (red, blue) PTV system with nozzle located at the left side of the image and flow from left to right: (a) red and blue light sheets made visible by piece of paper at camera plane of focus, and (b) cropped-view of particle flow through red/blue light sheets.

right, as shown in the image of Fig. 13a. Here, the exit of the nozzle is seen at the left of the image, and the adjacent red and blue light sheets are made visible with a piece of paper centered at the plane of focus of the camera system (note that the red light sheet appears yellow in the color camera's images, as there is some wavelength sensitivity overlap between the filters for the color channels). A cropped view of the particles passing through the two light sheets is shown in Fig. 13b, with particles illuminated by the red LED at the left and particles illuminated by the blue LED at the right. Some particles can be seen passing from the red sheet to the blue sheet within the duration of the LED pulse. However, it appears that the intensity decreases and then increases again during the particles' motion, which can be attributed to the non-uniformity of each light sheet over its width. This can be accounted for during calibration to provide a background intensity, which maps the intensity of the light sheets to each pixel prior to illumination of the particle flow. Note also that there are out-of-focus particles particularly in the blue illumination sheet, and these can be filtered using high-pass filtering of the images as described in Section 4.

A monochrome camera image of the two-color LED illumination is shown in Fig. 14a, where the rough position of the red and blue illumination sheets are depicted with the appropriately colored rectangles, and two streaks are identified, one in each light sheet. A Ronchi ruling (5 line pairs per millimeter) was used to obtain a spatial calibration of the image. The extracted intensity profile of each streak is shown with its respective color in the plot of Fig. 14b, with the simultaneously-measured photodiode profile for each shown in gray. The intensities of both the

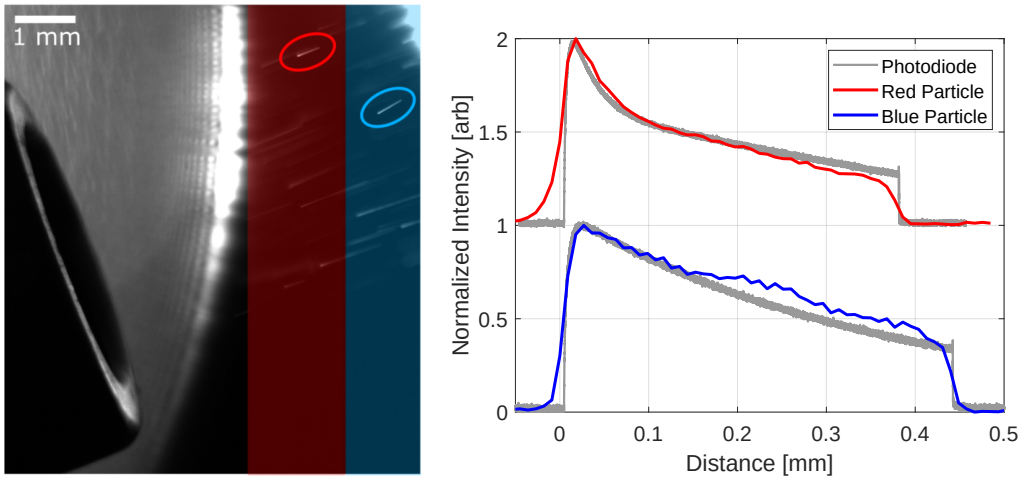

(a) (b)

Figure 14: (a) Two-color monochrome image from sideways-facing jet nozzle, with red and blue particles outlined in respective colors, and approximate location of the light sheets depicted with highlighted colored regions. (b) Normalized intensity decay profiles of red and blue particles with measured photodiode intensity decay signal from LEDs.

image profiles and the photodiode profiles are normalized between zero and unity for comparison purposes. Note that the distance traveled by the blue particle is slightly greater than the distance traveled by the red particle during the same pulse width duration of 300 μs, indicating that the blue particle has a larger velocity.

To extract quantitative information from this image, two methods can be used. The first is to identify the starting and ending points of each particle streak, and use the LED pulse width to determine the particles' velocities. The correct orientation of the particle streaks (the starting and ending points) are known due to the intensity decay direction, but this method discards information about the velocity and position of the particle along its path within the duration of the pulse width. From the streak data shown in Fig. 14b and using the pulse width of 300 μs, the velocities of the red and blue particle streaks are roughly 1.26 m/s and 1.47 m/s, respectively.

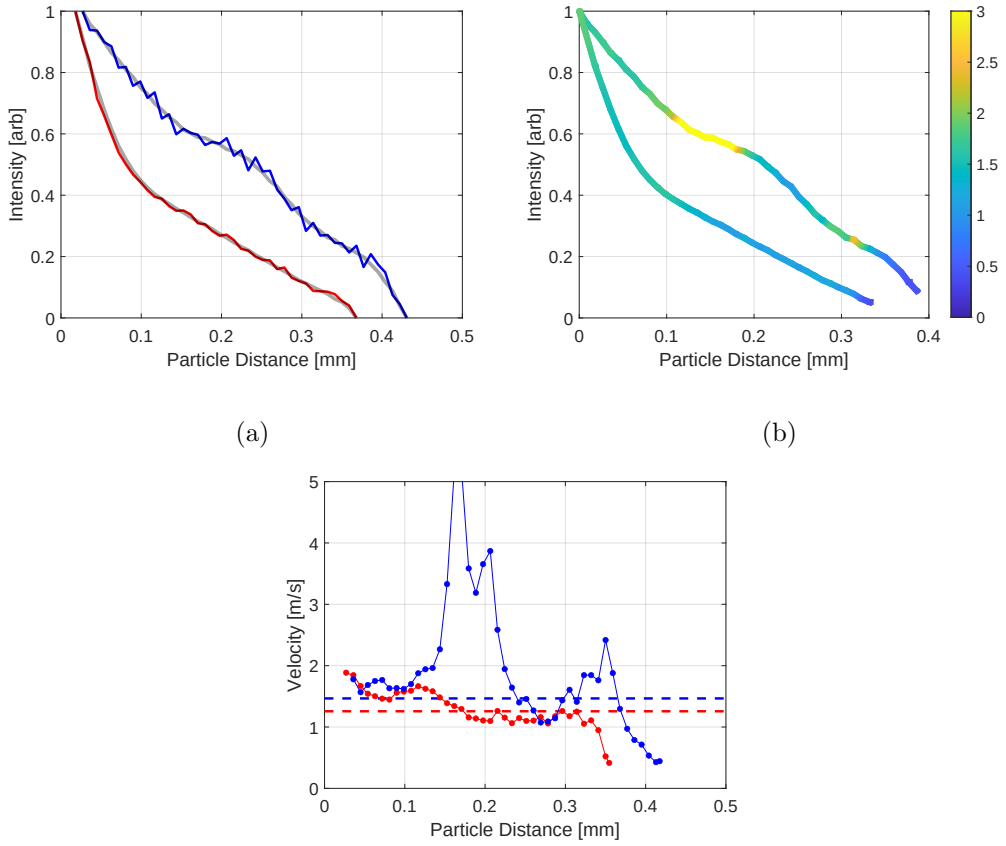

Figure 15: (a) Raw (color) and smoothed (gray) intensity decay profiles for red and blue particles corresponding to Fig. 14. (b) Sub-interval velocities for red and blue particles plotted along the intensity decay profile, colored by velocity in m/s. (c) Velocity of particle streak sub-intervals over particle distance, where dashed lines indicate mean streak velocity.

The second method of extracting quantitative information from the streak data is to discretize each streak into smaller sub-intervals to obtain a more finely-resolved estimate of both the particle velocity and direction along the streak. The two streaks from Fig. 14b are plotted again in Fig. 15a in their respective colors. Only the data from the starting point of the streak to the ending point are plotted, and intensities of the remaining data scaled between zero and unity. These data are smoothed slightly (gray data) to remove the small pixel-to-pixel intensity changes that are most visible in the blue profile. The smoothed streak profiles are then divided into smaller sub-intervals in time, and using the photodiode-monitored intensity decay profile in time, the velocity of the particle during each sub-interval is computed. The streak intensity decay profiles are plotted in Fig. 15b, and colored by the velocity of the particle in each sub-interval. The velocity of each sub-interval is also plotted versus particle distance in Fig. 15c. The red-illuminated particle moves at a roughly constant velocity, where the mean velocity computed over the full pulse width duration is indicated by the red dashed line in Fig. 15c. This roughly constant velocity of the red-illuminated particle also agrees with the results plotted in Fig. 14b, where the streak intensity decay profile from the image matches closely with that of the photodiode monitor. The blue-illuminated particle exhibits noisier velocity values using this sub-interval analysis, with velocities exceeding 5 m/s near the second quarter-interval of the streak. The first and third quarters of the streak generally fall within the 1 m/s to 2 m/s range, albeit with oscillations corresponding to the variation in the pixel intensity of the raw image which are then coupled into the analysis via the comparison to the smooth monitor photodiode decay profile. Different smoothing methods and sub-interval bounds can be used to increase the quality of the data, but these results demonstrate the general utility of the extraction of the velocity over the duration of the particle streak.

6 Conclusions

A PTV system was constructed which uses the inherent intensity decay from a low-cost LED and driving circuit to provide particle streak direction information and high spatial resolution particle velocity measurements. The use of an LED as the light source ensures the PTV system remains eye-safe, unlike similar measurements using a laser as the light source. Because the scattered intensity decay signal from the particles is captured in a single image frame, expensive dual-pulsing cameras and light sources are not needed; the camera's exposure for each frame must only be long enough to encompass the LED pulse width. The intensity decay of the LED illumination, dictated by the RC constant of the driving circuit, provides information about the directionality of the particles without actively modulating the intensity of the light as has been performed in earlier PTV systems. That is, this illumination strategy is passive as opposed to active, and requires only the desired pulse width of the entire streak to be dictated. Using two adjacent LED illumination regions and a single color camera can provide three-dimensional particle direction information by identifying in-plane particle direction using the intensity decay and out-of-plane motion by changes in the color of the scattered light from the particle.

Testing of both a single-color system and a two-color system was performed in the laboratory, using a small slow-speed jet seeded with approximately 1 μm particles. Qualitative comparisons of varying pulse widths of the LED illumination demonstrated that the system could be tailored for varying flow velocity regimes by changing the pulse width and associated camera single-frame exposure time. Using a two-color system with a color camera allowed for quick determination of particle illumination color and position. By replacing the color camera with a single monochrome camera, higher spatial resolution of the particle streaks was achieved (at the expense of a loss of wavelength sensitivity, which is important for three-component measurements), and velocity and position measurements of a red-illuminated and a blue-illuminated particle streak were made.

While the simple setup and operation is the primary benefit of this PTV system, there are aspects that may limit its usefulness in certain applications. The varying intensity of the light source's illumination over the camera's field-of-view must be accounted for before the accurate intensity decay profile can be definitively determined. While a pre-flow calibration image can be used for this purpose, this has not been demonstrated in this paper. Because the emitted light intensity from the LED units used in this paper is low compared with a typical laser source, a forward scattering imaging approach was used. The depth-of-focus of the imaged particles is determined by the camera system's depth-of-focus, which can be made quite narrow, on the order of a few millimeters. If using a side-scattering laser system, the imaging region depth is defined only by the laser sheet thickness, and the depth-of-focus of the imaging system can be larger. The forward-scattering orientation also results in out-of-focus particles that scatter the LED light, leading to larger particle streaks that affect the background signal, and which are then coupled into the intensity decay streaks of the in-focus particles. Lower seeding densities are desirable for this system to reduce the number of out-of-focus particles in the volume illumination configuration. In the phosphor decay PTV system, the imaged light is at a different wavelength than the incident light, and a bandpass filter can be used to eliminate the incident light intensity from the phosphorescence images. In the system described in this paper, the scattered light is of the same wavelength as the incident light, and spectral filtering cannot be used to eliminate unwanted signal. However, for simple imaging configurations, the LED intensity decay PTV system can prove useful. At minimum, the intensity decay of the illumination provides information about the direction of the particles, and using only the starting/ending points of the particle streak and the pulse width of the illumination source, the velocity of each particle can be computed, resulting in data similar to a conventional PIV system. With careful calibration of the light illumination prior to an experiment, high quality velocity data can be obtained, and with higher-intensity LED units, side-scattering configurations should be possible, mitigating some of the experimental setup and data processing challenges.

References

1. R. J. Adrian. Particle-Imaging Techniques for Experimental Fluid Mechanics. *Annual Review of Fluid Mechanics*, 23(1):261–304, January 1991.

2. J. Westerweel, G. E. Elsinga, and R. J. Adrian. Particle Image Velocimetry for Complex and Turbulent Flows. *Annual Review of Fluid Mechanics*, 45(1):409–436, January 2013.

3. M. Raffel, C. E. Willert, F. Scarano, C. J. Kähler, and S. T. Wereley. *Particle Image Velocimetry*. Springer-Verlag GmbH, April 2018.

4. T. W. Fahringer Jr. *On the Development of a Volumetric Velocimetry Technique using Multiple Plenoptic Cameras*. PhD Dissertation, Auburn University, December 2018.

5. O. Chételat and K. C. Kim. Miniature particle image velocimetry system with LED in-line illumination. *Measurement Science and Technology*, 13(7):1006–1013, June 2002.

6. J. Estevadeordal and L. Goss. PIV with LED: Particle Shadow Velocimetry (PSV) Technique. In *43rd AIAA Aerospace Sciences Meeting and Exhibit*. American Institute of Aeronautics and Astronautics, January 2005.

7. S. M. Hagsäter, C. H. Westergaard, H. Bruus, and J. P. Kutter. Investigations on LED illumination for micro-PIV including a novel front-lit configuration. *Experiments in Fluids*, 44(2):211–219, October 2008.

8. C. Willert, B. Stasicki, J. Klinner, and S. Moessner. Pulsed operation of high-power light emitting diodes for imaging flow velocimetry. *Measurement Science and Technology*, 21(7):075402, June 2010.

9. N. A. Buchmann, C. E. Willert, and J. Soria. Pulsed, high-power LED illumination for tomographic particle image velocimetry. *Experiments in Fluids*, 53(5):1545–1560, October 2012.

10. H. M. D. Harshani, S. A. Galindo-Torres, A. Scheuermann, and H. B. Muhlhaus. Experimental study of porous media flow using hydro-gel beads and LED based PIV. *Measurement Science and Technology*, 28(1):015902, December 2016.

11. M. P. Arroyo and C. A. Greated. Stereoscopic particle image velocimetry. *Measurement Science and Technology*, 2(12):1181–1186, December 1991.

12. C. Willert. Stereoscopic digital particle image velocimetry for application in wind tunnel flows. *Measurement Science and Technology*, 8(12):1465–1479, December 1997.

13. A. K. Prasad. Stereoscopic particle image velocimetry. *Experiments in Fluids*, 29(2):103–116, August 2000.

14. A. Schroeder and C. E. Willert. *Particle Image Velocimetry, New Developments and Recent Applications*. Springer Berlin Heidelberg, 2008.

15. T. Maxworthy. Discontinuity Properties of Laminar Flames. *Physics of Fluids*, 4(5):558–564, May 1961.

16. T. Maxworthy. Experiments on the Weis-Fogh mechanism of lift generation by insects in hovering flight. Part 1. Dynamics of the 'fling'. *Journal of Fluid Mechanics*, 93(1):47–63, July 1979.

17. K. A. Marko and L. Rimai. Video recording and quantitative analysis of seed particle track images in unsteady flows. *Applied Optics*, 24(21):3666, November 1985.

18. M. P. Wernet. Two-dimensional particle displacement tracking in particle imaging velocimetry. *Applied Optics*, 30(14):1839, May 1991.

19. M. P. Wernet and A. Pline. Particle displacement tracking technique and Cramer-Rao lower bound error in centroid estimates from CCD imagery. *Experiments in Fluids*, 15–15(4–5):295–307, September 1993.

20. T. D. Dickey and G. L. Mellor. Decaying turbulence in neutral and stratified fluids. *Journal of Fluid Mechanics*, 99(1):13–31, July 1980.

21. T. D. Dickey, B. Hartman, E. Hurst, and S. Isenogle. Measurement of fluid flow using streak photography. *American Journal of Physics*, 52(3):216–219, March 1984.

22. P. E. Dimotakis. Particle streak velocity field measurements in a two-dimensional mixing layer. *Physics of Fluids*, 24(6):995, 1981.

23. A. Cenedese and A. Paglialunga. A new technique for the determination of the third velocity component with PIV. *Experiments in Fluids*, 8(3-4):228–230, December 1989.

24. B. Khalighi and Y. H. Lee. Particle tracking velocimetry: an automatic image processing algorithm. *Applied Optics*, 28(20):4328, October 1989.

25. F. Dinkelacker, M. Schäfer, W. Ketterle, J. Wolfrum, W. Stolz, and J. Köhler. Determination of the third velocity component with PTA using an intensity graded light sheet. *Experiments in Fluids*, 13(5):357–359, September 1992.

26. M. Raffel, M. Gharib, O. Ronneberger, and J. Kompenhans. Feasibility study of three-dimensional PIV by correlating images of particles within parallel light sheet planes. *Experiments in Fluids*, 19(2):69–77, June 1995.

27. Ch. Brücker. 3-D PIV via spatial correlation in a color-coded light-sheet. *Experiments in Fluids*, 21(4):312–314, August 1996.

28. D. P. Towers, C. E. Towers, C. H. Buckberry, and M. Reeves. A colour PIV system employing fluorescent particles for two-phase flow measurements. *Measurement Science and Technology*, 10(9):824–830, August 1999.

29. M. Jehle and B. Jähne. A novel method for three-dimensional three-component analysis of flows close to free water surfaces. *Experiments in Fluids*, 44(3):469–480, January 2008.

30. J. M. Weisberger, B. F. Bathel, S. B. Jones, M. R. Woike, J. D. Ponder, J. T. Heineck, and E. T. Schairer. Preparations for Tomographic Background-Oriented Schlieren Measurements in the 11-by 11-Foot Transonic Wind Tunnel. In *AIAA Aviation 2020 Forum*. American Institute of Aeronautics and Astronautics, June 2020.

31. M. Raffel, J. N. Braukmann, C. E. Willert, L. Giuseppini, and C. C. Wolf. Feasibility study of in-line particle image velocimetry. *Experiments in Fluids*, 65(3), February 2024.

32. S. Someya, Y. Okura, M. Uchida, Y. Sato, and K. Okamoto. Combined velocity and temperature imaging of gas flow in an engine cylinder. *Optics Letters*, 37(23):4964, November 2012.

33. L. Fan, Y. Gao, A. Hayakawa, and S. Hochgreb. Simultaneous, two-camera, 2D gas-phase temperature and velocity measurements by thermographic particle image velocimetry with ZnO tracers. *Experiments in Fluids*, 58(4), March 2017.

34. T. Cai, J. Han, M. Kim, J. Jung, H. Shin, and K. C. Kim. Adaptive window technique for lifetime-based temperature and velocity simultaneous measurement using thermographic particle tracking velocimetry with a single camera. *Experiments in Fluids*, 63(10), October 2022.

35. B. Voss, J. Stapf, A. Berthe, and C. S. Garbe. Bichromatic particle streak velocimetry bPSV. *Experiments in Fluids*, 53(5):1405–1420, September 2012.

36. L. Fan, P. Vena, B. Savard, G. Xuan, and B. Fond. High-resolution velocimetry technique based on the decaying streaks of phosphor particles. *Optics Letters*, 46(3):641, January 2021.

37. L. Fan, P. Vena, B. Savard, and B. Fond. Experimental and numerical investigation on the accuracy of phosphor particle streak velocimetry. *Experiments in Fluids*, 63(10), October 2022.

38. C. D. Meinhart, S. T. Wereley, and M. H. B. Gray. Volume illumination for two-dimensional particle image velocimetry. *Measurement Science and Technology*, 11(6):809–814, May 2000.

39. S. Scharnowski and C. J. Kähler. Particle image velocimetry - Classical operating rules from today's perspective. *Optics and Lasers in Engineering*, 135:106185, December 2020.

40. B. M. Voss. *Novel single Camera Techniques for 3D3C Langrangian Trajectory Measurements in Interfacial Flows*. PhD thesis, Ruperto-Carola University of Heidelberg, May 2012.